Chemical reaction and diffusion kinetics during laser-induced submillisecond heating for lithographic applications

Jing Jiang, Byungki Jung, Michael O. Thompson, and Christopher K. Ober

Citation: Journal of Vacuum Science & Technology B 37, 041601 (2019); doi: 10.1116/1.5086871

View online: https://doi.org/10.1116/1.5086871

View Table of Contents: https://avs.scitation.org/toc/jvb/37/4

Published by the American Vacuum Society

ARTICLES YOU MAY BE INTERESTED IN

In situ liquid cell crystallization and imaging of thiamethoxam by helium ion microscopy Journal of Vacuum Science & Technology B **36**, 051803 (2018); https://doi.org/10.1116/1.5040849

Gas equilibration gas modulation refractometry for assessment of pressure with sub-ppm precision Journal of Vacuum Science & Technology B **37**, 042901 (2019); https://doi.org/10.1116/1.5090860

Comparative study of electron field emission from randomly-oriented and vertically-aligned carbon nanotubes synthesized on stainless steel substrates

Journal of Vacuum Science & Technology B 37, 041202 (2019); https://doi.org/10.1116/1.5098782

Wafer-scale fabrication of CMOS-compatible, high aspect ratio encapsulated nanochannels Journal of Vacuum Science & Technology B **36**, 051801 (2018); https://doi.org/10.1116/1.5034463

Review Article: Crystal alignment for high performance organic electronics devices

Journal of Vacuum Science & Technology A 37, 040801 (2019); https://doi.org/10.1116/1.5094904

Direct MBE growth of metamorphic nBn infrared photodetectors on 150 mm Ge-Si substrates for heterogeneous integration

Journal of Vacuum Science & Technology B 37, 031216 (2019); https://doi.org/10.1116/1.5088784





Chemical reaction and diffusion kinetics during laser-induced submillisecond heating for lithographic applications

Jing Jiang,¹ Byungki Jung,² Michael O. Thompson,² and Christopher K. Ober^{2,a)}
¹The Robert Frederick Smith School of Chemical and Biomolecular Engineering, Cornell University, Ithaca, New York 14853

(Received 24 December 2018; accepted 25 April 2019; published 5 June 2019)

Reactions in solid-state chemistry are controlled by both underlying chemical reaction rates and temperature-dependent diffusion of reactants and products. Due to distinctly different activation energies, the relative rates of reaction and diffusion may shift dramatically with temperature. In this work, the acid catalyzed deprotection of acid labile groups of model chemically amplified photopolymers was studied to understand the effects of temperature on diffusioncoupled reactions. In these systems, strong acids form during exposure of photoacid generators (PAGs) to ultraviolet radiation and then diffuse and catalyze deprotection reactions. By using very short duration laser-induced heating for the postexposure bake step, the potential reaction temperature range is extended by several hundred degrees compared to traditional thermal processing temperatures. Thermal degradation at these temperatures is avoided by simultaneously reducing the heating time from minutes to submilliseconds. Both diffusion and reaction rates were measured in this high temperature region for three different photoresists combined with two different PAGs, with activation energies of the key processes determined. The interplay of diffusion and reaction rates was also examined by comparing results of high-resolution pattern formation. The best image formation at high temperature was achieved using photoresists with high deprotection rates combined with PAGs exhibiting low diffusivity. Published by the AVS. https://doi.org/10.1116/1.5086871

I. INTRODUCTION

Photolithography remains the premier high-resolution patterning technique for not only integrated microelectronics manufacturing but also in many new applications such as engineered optics, 1-3 microelectro-mechanical systems, 4,5 and lab-on-a-chip devices. 5-7 The dominant chemistry of photolithography continues to be positive tone chemical amplification, ^{8,9} which involves a chemical deprotection step following the release of protons as acid catalyst during deep UV (DUV) exposure. The overall deprotection rate is determined by the relative rates of multiple underlying kinetic processes. As an example, deprotection requires diffusion of reactants to an active site followed by chain cleavage, with both rates typically increasing with temperature and following Arrhenius behavior. Depending on the activation energies, the relative rates may change markedly with temperature with different rate-limiting steps in low and high temperature regimes. In this study, we explored the effects of short time, high temperature excursions on model chemically amplified photoresists, relating the effects of the relative rates of diffusion and deprotection to changes in pattern transfer quality.

Thermal activation for chemical amplification is most commonly performed by heating films on minute time scales during the postexposure bake (PEB). Heating on significantly shorter timescales can be achieved using a number of techniques. For example, rapid thermal annealing (RTA) heats at rates up to 100 °C/s with temperatures held for 5–12 s before

cooling. ¹⁰ However, RTA is rarely used for organic materials such as polymers due to the temperature sensitivity of organic systems on the seconds timescale. At shorter timescales, our group has used laser spike annealing (LSA) to anneal polymers for millisecond and submillisecond times and have demonstrated that many polymers can withstand extreme temperatures, up to 800 °C in some cases, for these times. ^{11–14}

Understanding the temperature dependence of both acid diffusion and acid catalyzed deprotection is critical for photoresist design, especially for resist systems capable of achieving sub-10 nm dimensions. Diffusion of acid into unexposed regions is a key challenge and must be minimized to achieve high-resolution patterns with minimal image blur and pattern fidelity loss. 15 One path currently being explored involves designing resists with immobile photoacid generators (PAGs) chemically grafted to a photopolymer chain, ¹⁶ but this approach also comes at the cost of larger photopolymer size and the inability to iteratively improve process steps through the addition of separate photoactive compounds. 17,18 We believe that increasing the temperature, while simultaneously reducing the time, of the PEB may provide a route to limiting diffusion while providing an acceptable rate of deprotection. Such an approach would provide the opportunity for more molecular design flexibility of resist systems.

In recent works, we demonstrated the use of LSA as a PEB process (*l*-PEB) for conventional chemically amplified photoresists. ^{19–21} Using *l*-PEB, the effects of competing processes with changing relative rates were explored over a wide temperature range. In this paper, we show that the rational design of systems to fully exploit the benefits of *l*-PEB requires

²Department of Materials Science and Engineering, Cornell University, Ithaca, New York 14853

a)Electronic mail: cko3@cornell.edu

Fig. 1. Chemical structures of the photoresists synthesized on the same molecular weight polyhydroxystyrene with selectively varied side chains.

chemically amplified photoresists with low acid diffusivity coupled with high-deprotection-rate leaving groups.

II. EXPERIMENT

A. Photoresist and PAG design for laser and hotplate PEB

In order to study the effects of high temperature on deprotection, we synthesized several photoresists with a range of deprotection activation energies. Poly(hydroxystyrene) (PHS) of the same molecular weight (Sigma-Aldrich, 8000 g/mol) was used as a backbone in all cases as it has been extensively studied for 248 nm lithography9 and can be potentially used in 13.5 nm (EUV) lithography. 22-24 Unlike methacrylate backbones used for 193 nm lithography, PHS can incorporate a leaving group that is either a carbonate and a carboxylate ester. The leaving groups were consequently varied to cover a range of activation energies. Three different structures were synthesized for this study using *tert*-butoxy carbonate, tert-butyl methyloxy carboxylate, and methyl adamantyl units as protecting groups (referred to as t-BOC, t-BOCM, and AD, respectively) in Fig. 1. The t-BOC photoresist was chosen for its wide use in model chemically amplified photoresists over the past 30 years. The structure of t-BOCM is similar to t-BOC with the addition of a methyl group that separates the oxygen and carboxyl groups, decreasing the electronegativity of the leaving group and increasing the energy barrier to deprotection.²⁵ AD was chosen as a large alternative protecting group containing a carboxylate ester, realizing that the methyl adamantyl carbocation is somewhat less stable than the t-butyl carbocation, thereby increasing both the stability of the protected structure and deprotection activation energy. Since these three photopolymers were synthesized based on the same polymer backbone, their measured glass transition temperature Tg values were within 1 °C (Table S1).³⁷ It should be pointed out that these are model systems designed for our study and are not intended to be working photoresists, since these polymers consist of only one repeat function. Typical photoresists have 3–5 comonomers to tune exposure performance, development, pattern fidelity, and sensitivity.

Two PAGs were also investigated, a conventional triphenylsulfonium nonaflate (TPS-nf) as shown in Fig. 2(a) and a large PAG molecule, 2-(4-{1,1-bis[4-(1,1,2,2-tetrafluoro-2-sulfinoethoxy)phenyl]ethyl}phenoxy)-1,1,2,2-tetrafluoroethane1-sulfonate, referred to as 3P3A, synthesized for this study [Fig. 2(b)]. While 3P3A utilized the same TPS as the acid generating component, the counter ion, however, has three anions bound to a single trisphenol core. Such PAGs are known to be more environmentally friendly since the long fluorinated counter ions are partially replaced by phenolic groups. By increasing the total molecular weight of counter ions, acid diffusion is also reduced. The molecular weight per acid of the 3P3A was purposely chosen to be similar to TPS-nf so the same weight percentage of PAG should result in the same potential concentration of acid in the system.

B. Materials and reagents

Poly(4-vinylphenol) (Mn = 8 kg mol⁻¹; D = 1.4), 1,1, 1-Tris(4-hydroxyphenyl)ethane, propylene glycol methyl ether acetate (PGMEA), hexamethyldisilazane (HMDS), potassium carbonate, dimethylaminopyridine, TPS-nf, di-*tert*-butyl dicarbonate, and *tert*-butyl bromoacetate were purchased from Sigma-Aldrich and used without further purification. Ethyl acetate, acetone, tetrahydrofuran, hexanes, and toluene used in these reactions were HPLC grade from Fisher Scientific and used as received. Developer solution (0.26 N tetramethyl ammonium hydroxide in water,

(a) TPS-nf (b)
$$3P3A$$

Fig. 2. Chemical structure of the PAGs. These two PAGs have the same UV absorbing cation unit. TPS-nf is a common single activation site 248 nm PAG with a fluorinated counter ion, while 3P3A has three activation sites with three counter ions bound to a molecule glass core.

TMAH) from AZ electronic materials was used as received. 2-methyl-2-adamantyl bromoacetate was a gift obtained from Idemitsu Chemicals U.S.A. Corporation.

C. Synthesis

1. Synthesis of poly[4-(2-methyl-2-adamantyloxycarbonylmethoxy)styene-co-4-hydroxystyrene] (AD)

A mixture of 2-methyl-2-adamantyl bromoacetate (1.67 g, 5.8 mmol), poly(4-vinylphenol) (1 g, 0.125 mmol), and potassium carbonate (0.8 g, 5.8 mmol) was dissolved in tetrahydrofuran (30 ml). The mixture was heated to 66 °C and refluxed for 19 h. After cooling to room temperature, the mixture was filtered and evaporated under reduced pressure. The resulting powder was purified by silica gel column chromatography with a mixture of ethyl acetate and hexane. The resulting methyl adamantyl-substituted polymer powder was dried at 60 °C overnight under reduced pressure.

2. Synthesis of poly(4-t-butyloxycarbonylmethoxystyreneco-4-hydroxystyrene) (t-BOCM)

The synthesis followed the methodology outlined for the methyl adamantyl polymer using instead as reactants *tert*-butyl bromoacetate (1.3 g, 6.67 mmol), poly(4-vinylphenol) (1 g, 0.125 mmol), and potassium carbonate (0.92 g, 6.67 mmol).

3. Synthesis of poly(4-t-butyloxycarbonyloxystyrene-co-4-hydroxystyrene) (t-BOC)

Di-*tert*-butyl dicarbonate (0.64 g, 2.9 mmol) and dimethy-laminopyridine (0.048 g, 0.4 mmol) were added to a solution of poly(4-hydroxystyrene) (1 g, 0.125 mmol) in dry acetone. The solution was stirred at room temperature overnight and partitioned between ethyl acetate, brine, and 1 N HCl. The layers were separated, and the organic layer was washed with aqueous NaHCO₃, dried in Mg₂SO₄, and concentrated. The solvent was then evaporated and dried in a vacuum oven at 50 °C overnight; a 70% extent of protection reaction was achieved.

4. Synthesis of triphenylsulfonium 2-(4-{1,1-bis[4-(1,1,2,2-tetrafluoro-2-sulfinoethoxy)phenyl]ethyl} phenoxy)-1,1,2,2-tetrafluoroethane-1-sulfonate (3P3A)

The synthetic method was modified from the synthesis of 2-phenoxytetrafluoroethanesulfonate by Ramakrishnan Ayothi. ¹⁸ Instead of phenol, 1,1,1-tris(4-hydroxyphenyl)ethane was used as the starting material in order to synthesize the 3P3A.

D. Methods

¹H and ¹⁹F nuclear magnetic resonance (NMR) was performed at room temperature in a Varian INOVA400 spectrometer at the Cornell NMR facility. Spectra recorded in (CD₃)₂CO were referenced to internal tetramethylsilane (0 ppm) for proton spectra and to CF₃COOH (76.55 ppm) for fluorine spectra. Thermal analysis was performed with a TA Instruments Q500 thermal gravimetric analyzer at a heating rate of 10 °C/min under N₂ and a Q1000 differential scanning calorimeter at a ramp of 10 °C/min under N₂.

Either TPS-nf or 3P3A was added to the photoresist at 5 wt. % loading and dissolved in PGMEA. Films were spin coated onto HMDS primed wafers to a target thickness of 100 nm for DUV and E-beam exposures. The films were subjected to a postapply bake at 110 °C for 60 s. DUV exposure (λ = 254 nm) was carried out using an ABM contact aligner, and e-beam patterning was carried out using a JEOL 6300. For e-beam patterning, an accelerating voltage of 100 KV and a beam current of 250 pA were used. After the postexposure bake by hotplate or laser spike annealing, films were developed in 0.26 N TMAH solution for 60 s.

The film's thickness was determined using a Filmetrics F50-EXR measurement system. Scanning electron microscope images were taken using a Zeiss Ultra 55 SEM with lines parallel to the scanning direction. The resist samples were coated with a layer of Au/Pd to prevent charging. Line edge roughness and line width roughness (LWR) were calculated using the SUMMIT image analysis software (EUV technology, Martinez, CA).

The quantum yield of a PAG describes the efficiency of acid generation, specifically the number of acid molecules produced as a function of absorbed photons. The quantum yields of the new PAGs were measured by a method described by Pohlers *et al.*, ²⁶ using rhodamine B base as an indicator of the acid concentration (Fig. S1). ³⁷ As acid is introduced to the rhodamine solution, the lactone ring in the base structure is converted to a carboxylic acid, thereby changing the fluorescence properties of the dye. The intensity of the new acid peak is plotted as a function of UV exposure dose, and the slope of this line is used to calculate the quantum yield.

E. Thermal treatment

After exposure, photoresists were thermally treated using either a conventional hotplate PEB or the laser-induced *l*-PEB. For hotplate annealing, wafers were placed on an isothermal hotplate in air.

For *l*-PEB, a continuous-wave CO_2 laser ($\lambda = 10.6 \,\mu\text{m}$) was used to transiently heat samples for submillisecond to millisecond durations, with rapid temperature quenches, as thermal energy was conducted into unheated substrates. At the CO₂ wavelength, laser energy occurs by free-carrier absorption regime with heavily doped Si substrates ($\rho \sim 0.01-0.02 \Omega$ cm) used to ensure full absorption. The laser beam, focused to 90 by $700 \,\mu\text{m}^2$ Gaussian profiles, was scanned along its short axis. The heating duration, quantified as a dwell time, was controlled by the laser scan velocity (90-360 mm/s) and ranged from 250 to 1000 µs. The dwell is defined as the laser full-width-half-maximum (90 µm divided by the scan velocity) and is approximately the duration that the temperature remains above 90% of the peak temperature. To generate larger annealed areas for analysis, the laser beam was stitched by stepping orthogonal to the scan direction by $110 \,\mu m$ between scans. The peak temperature of the l-PEB at the wafer surface, a function of both dwell and power, was calibrated using thin film platinum thermistors and known Au melt and Si melt reference points.^{21,27}

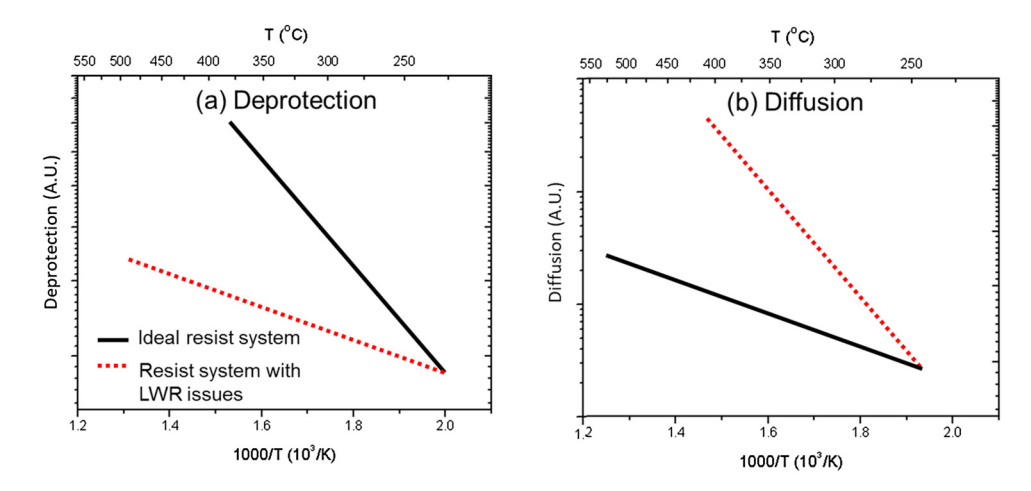


Fig. 3. Schematic Arrhenius plot of an ideal resist system for *l*-PEB exhibiting both (a) a high deprotection activation energy and (b) a low diffusion activation energy; under such conditions, short duration, high temperature anneals will preferentially deprotect the resist while minimizing acid diffusion.

III. RESULTS AND DISCUSSION

A. Background

Under hotplate PEB, previous studies have shown that high activation energies lead to lower LWR with only slight losses in resolution.²⁸ Extending this result to high temperature regimes, we would expect an *l*-PEB ideal system (Fig. 3) to exhibit a high deprotection activation energy with a low diffusion activation energy. The accelerated deprotection rate, relative to the diffusion, would minimize acid diffusion that is believed to be the primary source of LWR.

B. Avoiding thermolysis of photopolymers

At high temperatures, thermal cleavage of leaving groups from the backbone is a concern as it competes with acid catalyzed cleavage. Similar to acid deprotection, thermolysis during *l*-PEB is an activated process that depends on both temperature and well of the anneals. To understand this constraint, the thermal stability of these photopolymers without PAG was established to ensure that *l*-PEB was completed below any critical thermolysis temperature.

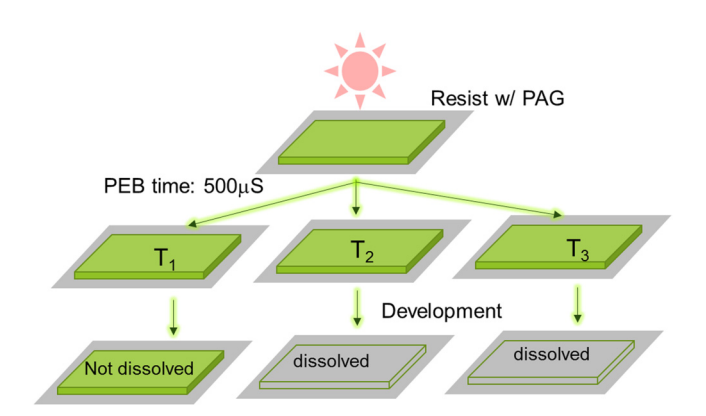
Thermal stability was determined by measuring the resist film thickness remaining after laser heating and development in the absence of any PAG. Films were annealed at increasing temperatures with a fixed dwell. At moderate temperatures (below decomposition of the backbone itself), side groups were thermally deprotected resulting in increased solubility and a film thickness decrease. The thermolysis temperature was, thus, determined as illustrated in Scheme 1. The reciprocal dwell time, a measure proportional to the effective reaction rate, is plotted as a function of inverse temperature (Arrhenius) to determine the activation energy and to establish the *l*-PEB operating temperature range for multiple dwell times (Fig. 4).

The activation energies for thermolysis are summarized in Table I. AD and t-BOCM have activation energies of 95 ± 10 and 86 ± 9 kJ/mol, respectively, while t-BOC has a slightly lower thermolysis activation energy of 77 ± 7 kJ/mol. It is worthwhile comparing the thermolysis activation energy with

deprotection energy as well as overall rate in order to understand the impact of acid and acid diffusion during *l*-PEB, which will be discussed below.

C. Characterization of deprotection during millisecond PEB

The acid deprotection rates, also measured using the method described in Scheme 1, are shown as an Arrhenius plot in Fig. 5 and were used to determine the deprotection activation energy with values summarized in Table I. Photoresist t-BOC, t-BOCM, and AD samples with 5 wt. % TPS-nf loading were exposed at a dose of $3.4 \, \text{mJ/cm}^2$, and deprotection activation energies were extracted from Fig. 5. This UV dose was chosen to remain in the dilute acid regime (14% PAG decomposition). As summarized in Table I, deprotection activation energies for t-BOC, t-BOCM, and AD are 58 ± 8 , 72 ± 5 , and $82 \pm 7 \, \text{kJ/mol}$, respectively. The deprotection activation energies of these photopolymers with



SCHEME 1. Method to determine the thermolysis and deprotection temperature for a given reaction time. For thermolysis, no PAG was added to the resist solution, while for acid deprotection, the PAG-containing resist is exposed to UV radiation at a fixed dose before *l*-PEB. As the peak temperature is increased, the film transitions from no dissolution to full dissolution during development. The lowest temperature required for full development is recorded as a function of heating duration, yielding an Arrhenius plot of the reaction rate vs temperature.

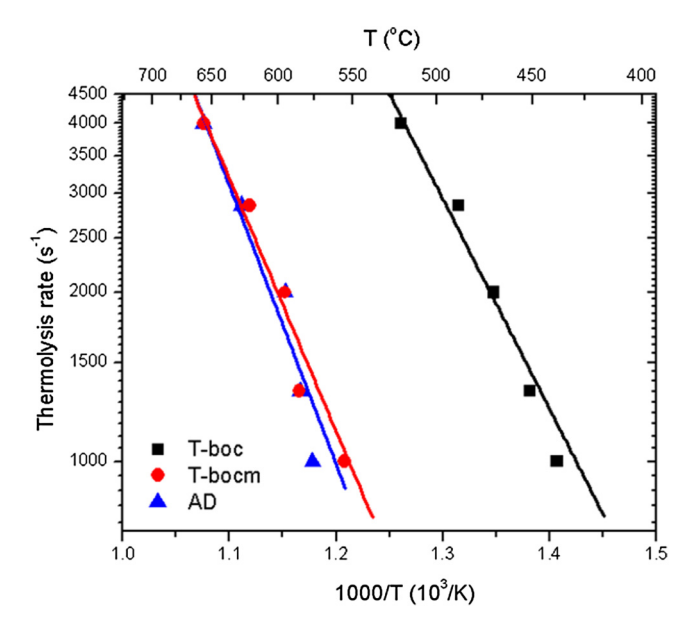


Fig. 4. Arrhenius thermolysis plot of t-BOC, t-BOCM, and AD under l-PEB.

TPS-nf show similar trends as expected during thermolysis since both thermolysis and acid deprotection share many similar elements in their reaction pathways. Compared to thermolysis, the presence of acid lowered the bond breaking activation energy of the carboxylate ester by ~20 kJ/mol and that of the carbonate ester by ~13 kJ/mol. While the activation energies of all three systems are comparable, the rates differ enormously as seen in Fig. 5. At the same temperature, the deprotection rate for the AD group is more than 2 orders of magnitude higher than the other systems (t-BOC and t-BOCM). Given a similar acid diffusion in all systems, this dramatically accelerated deprotection will result in reduced net diffusion and hence favor reduce image blur.

To study the effects of the initial acid concentration, we varied the exposure dose used to generate acid. The deprotection rate of the AD resist with TPS-nf PAG was investigated as a function of temperature at three different UV doses as shown in Fig. 6. As the UV exposure dose increased from 3.4 to 17.1 mJ/cm², the initial acid concentration level was calculated to increase from 14% to 53% of the total

TABLE I. Thermolysis, deprotection, and diffusion activation energies.

Resist	PAG ^a	Thermolysis Ea (kJ/mol)	Deprotection Ea (kJ/mol)	Diffusion Ea (kJ/mol)	
t-BOC	TPS-nf	77 ± 7	58 ± 8	400 ± 80	
t-BOCM	TPS-nf	86 ± 9	72 ± 5	302 ± 6	
AD	TPS-nf	95 ± 10	82 ± 7	280 ± 57	
AD	3P3A	N.A.	77 ± 6	195 ± 10	

^aNo PAG was added to the photoresist for thermolysis experiments. PAG loading for deprotection and diffusion experiments was 5 wt. % of the solid. Deprotection experiments were performed at 3.4 mJ/cm² DUV exposure, while the diffusion experiments were performed at 34 mJ/cm². Uncertainties in activation energy are the standard error.

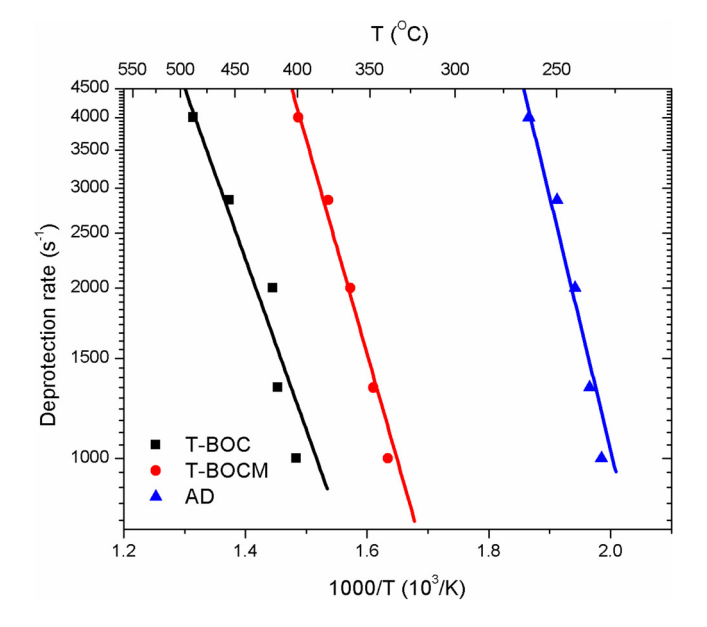


Fig. 5. Arrhenius deprotection plot of t-BOC, t-BOCM, and AD under *l*-PEB. The resists were loaded with 5 wt. % TPS-nf and exposed at 248 nm for 3.4 mJ/cm².

PAG loading by using Dill's equation. ²⁹ The activation energies for these three exposure levels, 82 ± 7 , 88 ± 11 , and 74 ± 15 kJ/mol, respectively, were nearly independent of exposure dose. When the acid concentration was doubled (14% at 3.4 mJ/cm², 25.3% at 6.8 mJ/cm², and 53% at 17.7 mJ/cm²), the deprotection rate increased by four times for TPS-nf, suggesting that a non-first-order reaction may be occurring during laser-induced heating. This behavior was also observed in previous studies of another adamantyl protected resist, ²⁷ which later was found by NMR study to originate from the formation of a unique decomposition product. ²¹

We also performed deprotection studies of AD with 5 wt. % 3P3A loading. We observed that the absolute deprotection rate increased with an increase of the initial acid concentration, but that the deprotection activation energy $(75 \pm 5, 83 \pm 8, \text{ and } 72 \pm 1 \text{ kJ/mol})$ changed by only 6% over a factor of 3 change in exposure dose. These activation energies were consistently lower than those observed for the other systems.

Comparing two different PAGs in the same resist matrix, the deprotection rates varied enormously despite similar deprotection activation energies. The activation energy is primarily related to the resist chemistry and, since the resist/ photoacid decomposition chemistry is the same, the activation energy was not expected to vary significantly at different exposure doses or for different PAG species, as observed. The crucial factor that determines the deprotection rate is the overall reaction rate. Quantum yield analysis showed that both TPS-nf and 3P3A have similar acid yields from the same exposure dose in acetonitrile solution. Since the acid yield is impacted by the surrounding medium, the absolute quantum yield in a thin film during e-beam and DUV exposure could be different. We believe that the two PAGs generated comparable initial concentrations of acid catalyst before l-PEB (Fig. S1).37 The trifunctional PAG, 3P3A, has lower diffusivity than TPS-nf, which will be discussed below.

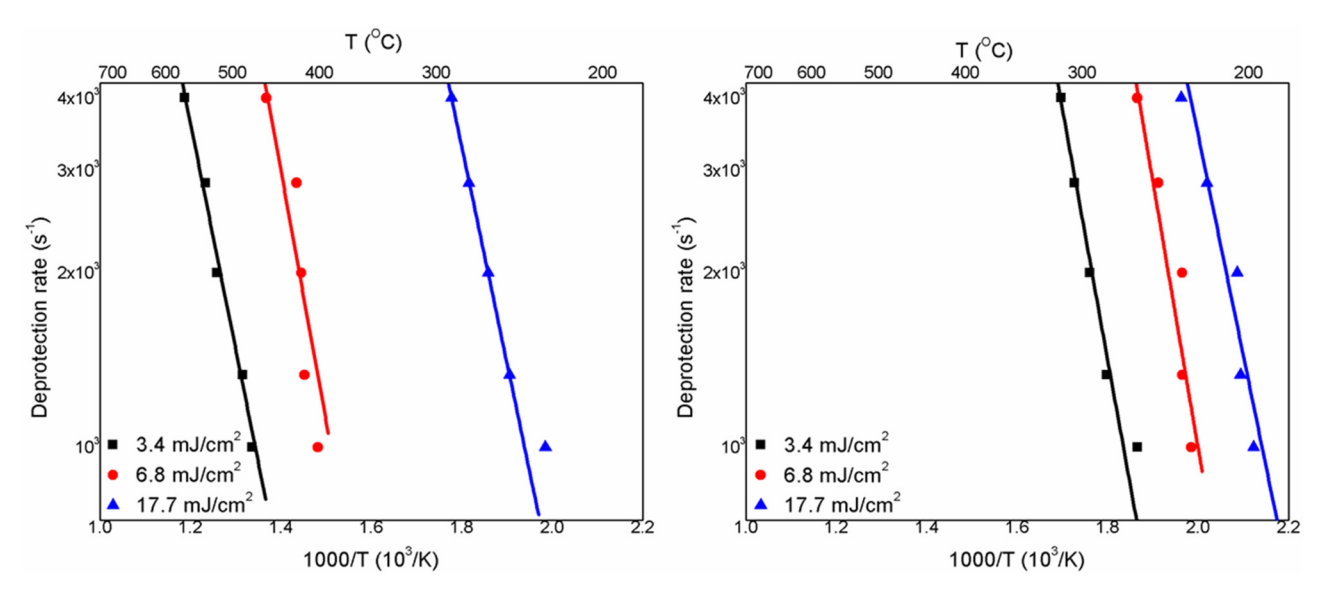


Fig. 6. Arrhenius deprotection plot of AD with (a) TPS-nf and (b) 3P3A at three doses under l-PEB. The deprotection activation energies from low and high doses are (a) 82 ± 7 , 88 ± 11 , and 74 ± 15 kJ/mol and (b) 75 ± 5 , 83 ± 8 , and 72 ± 1 kJ/mol. At a low dose, fewer acid groups are generated and hence higher temperatures are required to increase the diffusion and complete the deprotection within the given annealing time. However, the deprotection activation energy is primarily dependent on the resist chemistry and only weakly dependent on UV dose or the specific PAG.

D. Characterization of acid diffusivity

During UV patterning, a large gradient in acid concentration is generated at the pattern edges. Acids formed in the exposed areas can diffuse laterally into the unexposed areas leading to resist blur and line edge roughness. A resist bilayer structure was used to quantify this acid diffusion (Fig. S2). 30,37 The top layer consisted of a PAG-containing resist, while the bottom layer was an equivalent PAG-free made resist resin. The bilayers were flood exposed to generate acids in the surface layer. During PEB, deprotection and the resulting solubility change should occur only within the PAG-containing top layer; however, as acids diffuse to the PAG-free bottom layer and induce deprotection, part of the bottom layer near the interface also becomes soluble. After development, the thickness loss of the bottom layer was measured to determine the acid diffusion distance and the effective diffusivity at different annealing temperatures.

The acid diffusivity of TPS-nf in AD, t-BOC, and t-BOCM photopolymers is plotted as a function of reciprocal temperature in Fig. 7, and the activation energies are summarized in Table I. The highest diffusion activation energy was observed in t-BOC while AD exhibited the lowest. Thus, although the deprotection rate is fastest with t-BOC, the diffusivity is higher as well and t-BOC photoresists are more prone to image damage. And while the deprotection rate is slow with AD, diffusivity is low and this resist is less prone to image blurring.

Acid transport is strongly dependent on concentration, dynamic-free volume, and acid trapping mechanisms.³¹ In the t-BOC system, for example, the film density doubles after PEB due to the evaporation of volatile byproducts including carbon dioxide and isobutylene.³² The increased film density reduces acid transport in the deprotected t-BOC matrix. In contrast, nonvolatile byproducts such as methylene adamantine are formed by the deprotection of

AD leading to minimal changes in film density during PEB.²¹ However, these remaining byproducts may act as plasticizers, decreasing the energy barrier for acid diffusion in AD.

Ultimately, the diffusivity of the proton is closely related to the diffusivity of the counter ions as they must diffuse in the resist as a pair to maintain local charge neutrality. Previous reports have shown that attaching the anion to the polymer backbone greatly reduces the acid diffusion length.³³ Our results similarly show that anchoring three anions to a trisphenol core is effective in reducing the acid diffusivity (Fig. 8).

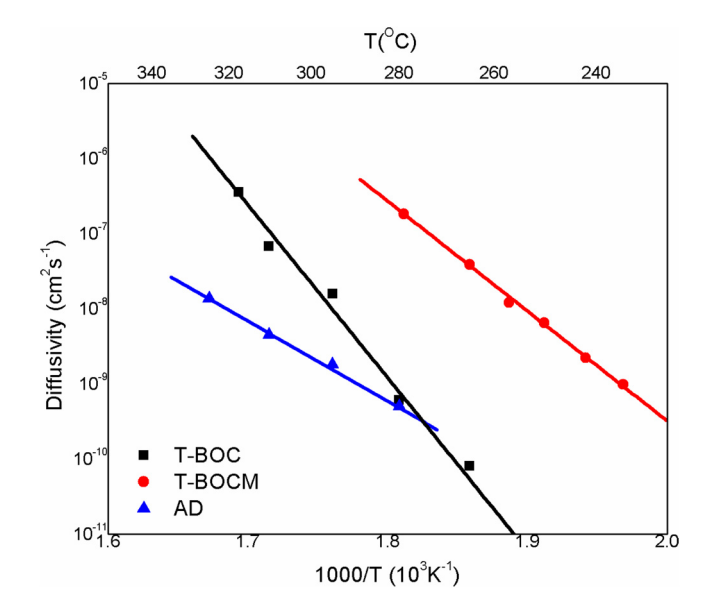


Fig. 7. Arrhenius plot of acid diffusivity, determined using a bilayer technique, of TPS-nf in three resist resins t-BOC, t-BOCM, and AD under *l*-PEB. The resist film was flood exposed at 248 nm for 34 mJ/cm², activating 90% of the PAG.

E. E-beam patterning and line width roughness of the resists

The deprotection and diffusion in an exposed resist at the exposure edge can be quantified as the latent image log slope (LILS), which is inversely proportional to the line edge roughness.³⁴ LILS is affected by the acid diffusivity, deprotection rate, and initial acid concentration. High diffusivity leads to a faster broadening of the reaction-diffusion front. In contrast, high deprotection rates not only kinetically trap acids but also modify resist polarity making diffusion more difficult.³⁵ Previous studies have found that, within 1.2 nm of the interface, there is a highly deprotected region where the acids are kinetically trapped. Beyond this 1.2 nm zone, the acid concentration decreases to a level where the extent of deprotection is at or below the polarity switch.³⁵ This variable distance deprotection is a main source of roughness. The extent of reaction is also strongly affected by the local acid concentration, as high initial acid concentration can induce more deprotection reactions.

It should be noted that we have not explicitly addressed the concept of catalytic chain length in these photoresists, since the proton catalyzed deprotection reaction depends on PAG concentration and diffusion distance in *l*-PEB just as it does in hotplate PEB. PAG efficiency can be considered to be the same in all experiments. Two avenues we can use to control acid diffusion distance are through the use of trifunctional PAGs in place of monofunctional PAGs (large PAG diffuses less) and by dwell time control of the *l*-PEB step (shorter time heating time above Tg gives shorter diffusion time). More important in *l*-PEB is the effect of high temperature on the relative rate of diffusion versus deprotection, the consequences of which are seen below.

In order to create a sharp acid concentration gradient and evaluate how deprotection and diffusion affect LILS and LWR, we used electron beam exposure to pattern these resists.

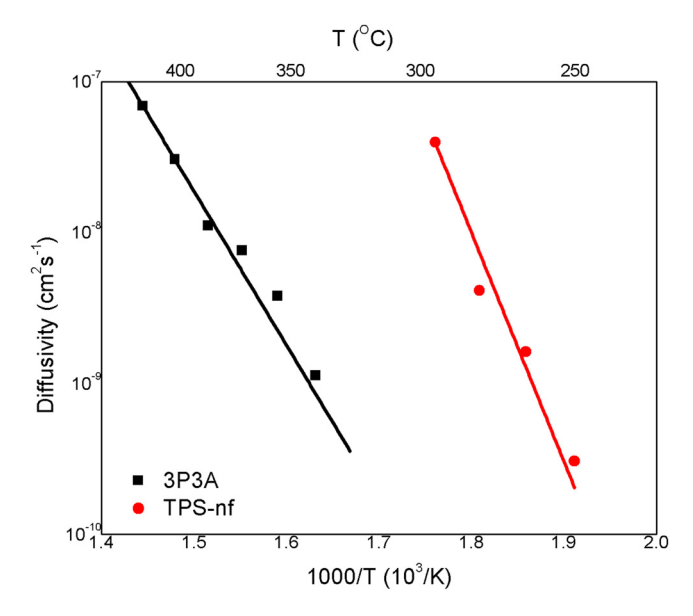


Fig. 8. Arrhenius plot of acid diffusivity of TPS-nf and 3P3A in AD resist resin under *l*-PEB. The resist film was flood exposed at 248 nm for 34 mJ/cm². The diffusivity is much lower for the 3P3A PAG in this matrix.

Despite reports that both deprotection and crosslinking of PHS occur during e-beam exposure, the overall mechanism for acid catalyzed deprotection by e-beam radiation is believed to be comparable to that produced by DUV exposure. The PEB time of hotplate and laser heating were fixed to 60 s and 500 μ s, respectively, while the PEB temperatures and exposure doses were varied. To avoid the influence of variations of acid concentration on patterning, a fixed dose for each resist system was finally chosen for the comparison between l-PEB and hotplate PEB. SEM images of e-beam patterning using three resists with TPS-nf are shown in Figs. 9(a)–9(f), and their patterning results are summarized in Table II.

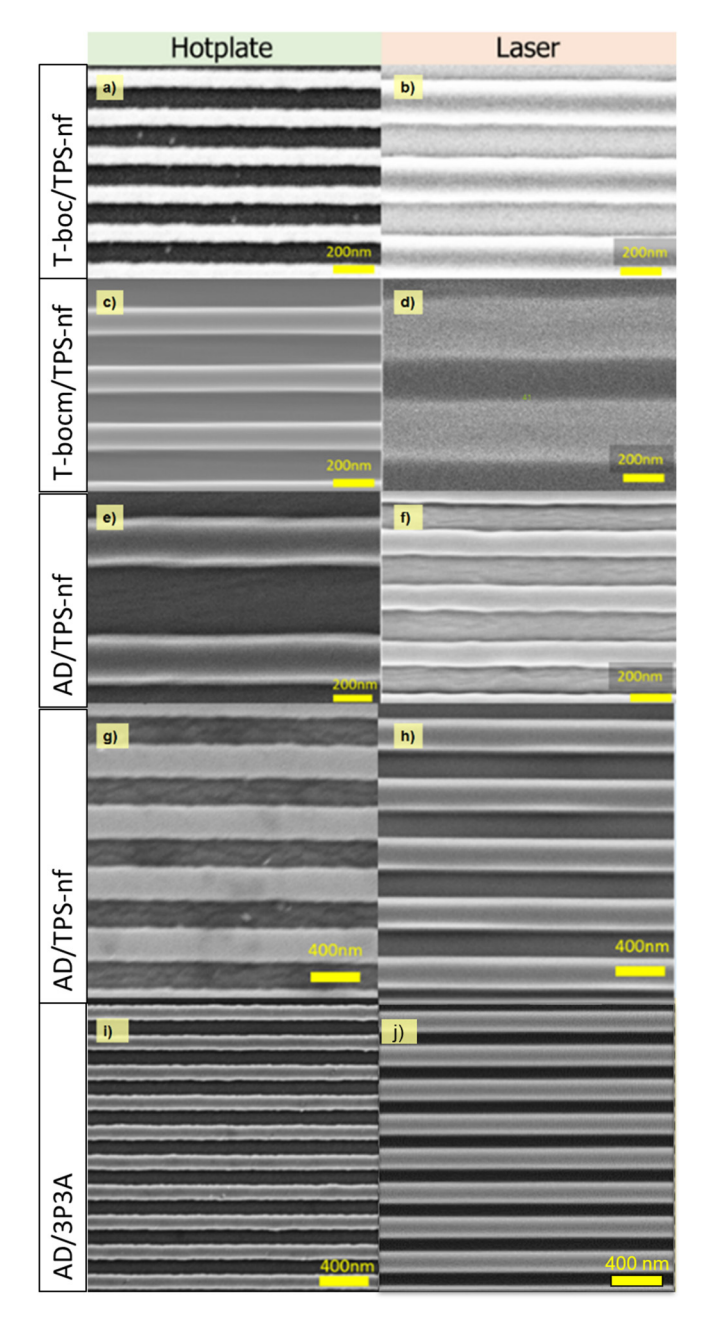


Fig. 9. SEM images of e-beam lithography showing the highest resolution obtained under each condition. Images on the left underwent hotplate PEB and images on the right underwent *l*-PEB. Patterning condition and results are summarized in Table II.

TABLE II. Patterning conditions and results using e-beam lithography.

			Hotplate (115 °C 60 s)			Laser (500 µs)		
	Resist	PAG	Dose (μC/cm ²)	CD (nm)	LWR (nm)	Dose (μ C/cm ²)	CD (nm)	LWR (nm)
Figures 9(a) and 9(b)	t-BOC	TPS-nf	15	99 ± 3	9.8 ± 0.1	20	204 ± 3	35 ± 0.7
Figures 9(c) and 9(d)	t-BOCM	TPS-nf	70	141 ± 4	9.7 ± 0.2	70	282 ± 5	21.3 ± 0.5
Figures 9(e) and 9(f)	AD	TPS-nf	45	249 ± 5	16.5 ± 0.3	45	141 ± 2	14.2 ± 0.4
Figures 9(g) and 9(h)	AD ^a	TPS-nf	30	222 ± 5	20 ± 0.5	60	216 ± 4	8.7 ± 0.1
Figures 9(i) and 9(j)	AD	3P3A	120	106 ± 3	10.2 ± 0.2	120	123 ± 2	3.5 ± 0.1

^aAll *l*-PEB was performed at 295 °C except for image (h) at 265 °C.

The resolution limit of each photopolymer system was examined by e-beam lithography at 50–100 nm pitch with 10 nm step, 100–200 nm with 25 nm step, and 200 nm and above with 50 nm step with 0.5 duty cycle. Each image shows the highest resolution pattern that was achieved under a given set of PEB conditions. Similar to previous reports, ²⁸ pattern collapse is observed at smaller dimensions. Using our model photoresists in combination with monofunctional and trifunctional PAGS, we focused on the study of LSA impact on LWR and the effect of leaving group type and PAG diffusivity on *l*-PEB effectiveness.

Under hotplate annealing, resolution of the t-BOC and t-BOCM systems was approximately 100 and 150 nm, respectively, with an LWR of approximately 10 nm. Under *l*-PEB, the resolution was 200 and 300 nm with an LWR of 35 and 21 nm, respectively. We believe the increase of LWR and the failure of sub-200 nm patterning is due to the accelerated acid diffusion at high temperature resulting from the high diffusion activation energy. As diffusion increases, LILS decreases and LWR becomes more pronounced.

In contrast, AD with its high deprotection activation energy and associated rates maintains high resolution with a slight decrease (from 16.5 to 14.2 nm) in LWR during *l*-PEB. This is possibly a result of maintaining the relative rates of deprotection rate and diffusivity even at high temperature. Therefore, the AD resist was the focus of further studies to achieve better patterning results using *l*-PEB.

Combined with AD, both TPS-nf and 3P3A demonstrated reduced LWR using *l*-PEB as seen in Figs. 9(g)-9(j). The roughness of patterns using TPS-nf in AD is further reduced at 265 °C (8.7 nm) compared to 295 °C (14.2 nm) but requires a higher dose. When the dose is fixed for AD with 3P3A, a 60% reduction in roughness (from 10.2 ± 0.2 to 3.5 ± 0.1 nm) is achieved using *l*-PEB compared to the conventional PEB at 115 °C. Due to the low acid diffusivity and low diffusion activation energy, the acid generated upon exposure is largely confined to the local exposure area and a much higher dose is required in order to achieve the same extent of deprotection. While 3P3A has the lowest diffusivity, its diffusion activation energy is also low. Consequently, the diffusivity changes slowly with increasing temperature during laser annealing. The photopolymer AD also has a high deprotection activation energy, which leads to the rapid increase in the deprotection rate; thus, LILS increases and the LWR is reduced by using *l*-PEB. This is consistent with a previous study which evaluated resists with low and high activation energies using conventional hotplate PEB.

IV. SUMMARY AND CONCLUSIONS

The effect of submillisecond laser spike and hotplate thermal annealing on both photopolymer deprotection and the accompanying acid diffusion was studied in model systems. Three different photopolymers with different protecting groups to tune the deprotection reaction rates were used in combination with two photoacid generators to alter acid diffusion. The deprotection activation and diffusion activation energies were measured and correlated to the line width roughness during electron beam patterning. The model resist with t-boc protecting groups had the best patterning performance in terms of resolution under hotplate PEB conditions. When *l*-PEB was used with this polymer, the performance was not nearly as good. However, the AD resist system, with its strong deprotection rate dependence on temperature, exhibited the best line width roughness under l-PEB, confirming that deprotection can be made to dominate at high temperature. Photoresist AD combined with slow diffusing 3P3A yielded the best performing PAG-resist pair with a 60% reduction in edge roughness achieved relative to conventional PEB conditions at a constant exposure dose. This work not only demonstrates how the temperature dependence of reaction rate simultaneously impacts competing processes at high temperature but it also provides a guide for the use of extreme, short time temperatures to balance competing chemical reactions. For a resist system to benefit from l-PEB, it should have a high deprotection activation energy (strong temperature dependence on deprotection) and low diffusion activation energy (weak temperature dependence on diffusion) to suppress excessive acid diffusion during high temperature PEBs. The AD resist combined with 3P3A shows that this is indeed possible and suggests a molecular design strategy to further improve resist performance. Given that these are only model homopolymer photoresists, these results also demonstrate the very real improvements possible in patterning performance using *l*-PEB, where better optimized resist systems with the appropriate characteristics should be able to surpass the imaging achieved using conventional PEB methods.

ACKNOWLEDGMENTS

The work at Cornell was supported by GlobalFoundries through the Semiconductor Research Corporation (Task IDs: 2137.001 and 2137.002). The authors gratefully acknowledge Kenji Yoshimoto for helpful discussions and critical assistance. This work made use of the Cornell Center for Materials Research Shared Facilities, which are supported through the NSF MRSEC program (No. DMR-1719875), and this work was performed in large part at the Cornell NanoScale Science & Technology Facility (CNF), a member of the National Nanotechnology Coordinated Infrastructure (NNCI), which is supported by the National Science Foundation (NSF) (Grant No. DMR-1719875).

- ¹Y. Chen, Microelectron. Eng. **135**, 57 (2015).
- ²M. Khorasaninejad and F. Capasso, Science **358**, eaam8100 (2017).
- ³M. Khorasaninejad, W. T. Chen, R. C. Devlin, J. Oh, A. Y. Zhu, and F. Capasso, Science **352**, 1190 (2016).
- ⁴J. W. Judy, Smart Mater. Struct. **10**, 1115 (2001).
- ⁵A. Pimpin and W. Srituravanich, Eng. J. 16, 37 (2011).
- ⁶D. Figeys and D. Pinto, Anal. Chem. **72**, 330 A (2000).
- ⁷D. Mijatovic, J. C. T. Eijkel, and A. van den Berg, Lab Chip **5**, 492 (2005).
- ⁸H. Ito, Chemical Amplification Resists for Microlithography (Springer, Berlin 2005)
- ⁹E. Reichmanis, F. M. Houlihan, O. Nalamasu, and T. X. Neenan, in *Polymers of Microelectronics*, edited by L. Thompson, C. G. Willson, and S. Tagawa (American Chemical Society, Washington, DC, 1993), pp. 2–24.
- ¹⁰J. Narayan, O. W. Holland, R. E. Eby, J. J. Wortman, V. Ozguz, and G. A. Rozgonyi, Appl. Phys. Lett. 43, 957 (1983).
- ¹¹B. Jung, C. K. Ober, M. O. Thompson, T. R. Younkin, and M. Chandhok, Proc. SPIE **7972**, 79722S (2011).
- ¹²J. Jiang, B. Jung, M. O. Thompson, and C. K. Ober, Proc. SPIE 8682, 86821N (2013).
- ¹³J. Jiang, A. G. Jacobs, B. Wenning, C. Liedel, M. O. Thompson, and C. K. Ober, ACS Appl. Mater. Interfaces 9, 31317 (2017).
- ¹⁴J. Jiang, A. Jacobs, M. O. Thompson, and C. K. Ober, J. Photopolym. Sci. Technol. 28, 631 (2015).

- ¹⁵J. Sha, J.-K. K. Lee, S. H. Kang, V. M. Prabhu, C. L. Soles, P. V. Bonnesen, and C. K. Ober, Chem. Mater. 22, 3093 (2010).
- ¹⁶Sang-Tae Kim, Ki-Ho Baik, Min-Ho Jung, and Kwang-Duk Ahn, Polym. Bull. 39, 423 (1997).
- ¹⁷R. A. Lawson, C.-T. Lee, R. Whetsell, W. Yueh, J. Roberts, L. Tolbert, and C. L. Henderson, Proc. SPIE 6519, 65191N (2007).
- ¹⁸R. Ayothi, H. B. Cao, W. Yueh, S. Putna, and C. K. Ober, Chem. Mater. 19, 1434 (2007).
- ¹⁹J. Sha, B. Jung, M. O. Thompson, C. K. Ober, M. Chandhok, and T. R. Younkin, J. Vac. Sci. Technol. B 27, 3020 (2009).
- ²⁰M. Krysak, B. Jung, M. O. Thompson, and C. K. Ober, Proc. SPIE 8325, 83250M (2012).
- ²¹B. Jung, P. Satish, D. N. Bunck, W. R. Dichtel, C. K. Ober, and M. O. Thompson, ACS Nano 8, 5746 (2014).
- ²²A. Narasimhan, S. Grzeskowiak, C. Ackerman, T. Flynn, G. Denbeaux, and R. L. Brainard, Proc. SPIE 10143, 101430W (2017).
- ²³S. Grzeskowiak, G. H. Denbeaux, R. L. Brainard, J. Kaminsky, M. Murphy, S. Gibbons, and J. Chandonait, Proc. SPIE 10586, 105860D (2018).
- ²⁴T. Sato, Y. Togashi, S. Shinjo, T. Toida, M. Echigo, and T. Makinoshima, Proc. SPIE **10809**, 108091X (2018).
- ²⁵S. A. MacDonald, C. G. Willson, J. M. J. Frechet, A. Macdonald, C. Grant, and M. J. Frechets, Acc. Chem. Res. 27, 151 (1994).
- ²⁶G. Pohlers, J. C. Scaiano, and R. Sinta, Chem. Mater. **9**, 3222 (1997).
- ²⁷B. Jung, J. Sha, F. Paredes, M. Chandhok, T. R. Younkin, U. Wiesner, C. K. Ober, and M. O. Thompson, ACS Nano 6, 5830 (2012).
- ²⁸J. W. Thackeray, R. A. Nassar, K. Spear-Alfonso, T. Wallow, and B. LaFontaine, J. Photopolym. Sci. Technol. 19, 525 (2006).
- ²⁹J. H. Liu and J. C. Shih, Macromol. Chem. Phys. **202**, 2986 (2001).
- ³⁰S. H. Kang, W. L. Wu, K.-W. W. Choi, A. De Silva, C. K. Ober, and V. M. Prabhu, Macromolecules **43**, 4275 (2010).
- ³¹M. D. Stewart, H. V. Tran, G. M. Schmid, T. B. Stachowiak, D. J. Becker, and C. G. Willson, J. Vac. Sci. Technol. B 20, 2946 (2002).
- ³²M. D. Stewart, M. H. Somervell, H. V. Tran, S. V. Postnikov, and C. G. Willson, Proc. SPIE 3999, 665 (2000).
- ³³M. Wang, N. D. Jarnagin, C.-T. Lee, C. L. Henderson, W. Yueh, J. M. Roberts, and K. E. Gonsalves, J. Mater. Chem. 16, 3701 (2006).
- ³⁴V. M. Prabhu, S. Kang, D. L. VanderHart, S. K. Satija, E. K. Lin, and W. Wu, Adv. Mater. 23, 388 (2011).
- ³⁵E. Croffie, M. Cheng, and A. Neureuther, J. Vac. Sci. Technol. B **17** (1999).
- ³⁶S. Enomoto, A. Oshima, and S. Tagawa, Proc. SPIE **8679**, 86792C (2013).
- ³⁷See supplementary material at https://doi.org/10.1116/1.5086871 for information about the thermal characteristics of the model photoresists used in these studies and the quantum yield of the two PAGs.